The Holocene 10,6 (2000) pp. 703–718

Bransfield Basin fine-grained sediments: late-Holocene sedimentary processes and Antarctic oceanographic conditions

J. Fabrés,[1] A. Calafat,[1]* M. Canals,[1] M.A. Bárcena[2] and J.A. Flores[2]

([1]G.R.C. Geociències Marines, Departament d'Estratigrafia i Paleontologia, Universitat de Barcelona, Campus Universitari de Pebralbes, E-08028 Barcelona, Spain; [2]Departamento de Geología, Facultad de Ciencias, Universidad de Salamanca, E-37008 Salamanca, Spain)

Received 28 July 1999; revised manuscript accepted 24 February 2000

A HOLOCENE RESEARCH PAPER

Abstract: The Antarctic Peninsula is sensitive to climatic change due to its northerly position and to the relatively reduced volume and character of its ice cover. High-resolution palaeoclimatic records from the Antarctic Peninsula ice cores extend back only 500 years. A climatic record of 2850 years in the Bransfield Basin is investigated through the analysis of sediment gravity cores from the floor of the central subbasin (core GEBRA-1) and the slope of the eastern subbasin (core GEBRA-2). Sedimentological, mineralogical and geochemical properties have been systematically measured, together with Accelerator Mass Spectrometry (AMS) radiocarbon dating. The fine-grained sediments result from two main processes: hemipelagic settling from resuspensions and primary productivity, and turbidity currents. Hemipelagic sediments were selected to investigate the oceanographic and climatic conditions of the northern Antarctic Peninsula region during the last three millennia. Cold climatic periods are characterized by millimetric laminations and/or black layers with higher organic carbon, nitrogen and opal contents. Warm periods are recorded as massive to diffuse laminated facies with lower biogenic contents. The results include the 'Little Ice Age' (LIA) cold pulse as well as several 200–300 year long fluctuations within the LIA and before this major climatic event of the Holocene.

Key words: Bransfield Basin, late Holocene, marine sedimentology, geochemistry, palaeoceanography, palaeoclimatology, Antarctic.

Introduction

The increased interest in past climatic conditions, due to the need for an understanding of global climate and its fluctuations, has made possible the collection of palaeoclimatic records of different origin around the world. Detailed stratigraphy of deep-sea sediment cores can provide information about palaeoceanographic aspects linked with climate evolution. Interest in the interpretation of the deep-sea sediment record in Antarctic Peninsula (AP) area is given by: (a) the environmental and ecological sensitivity of high-latitude areas covered by small ice caps to climatic change (Crowley and Baum, 1995); (b) the simple and high-speed response of those ice caps to climatic fluctuations (Barker *et al.*, 1998); and finally (c) the lack of other kinds of high-resolution climatic records from this area for the last few thousand years (Leventer *et al.*, 1996).

A key point in palaeoenvironmental reconstructions from marine sedimentary records is discriminating the different processes that control sedimentary particle deposition on the sea floor. The accurate determination of the contribution of each process is essential to assess the type and quality of the palaeoenvironmental information that will be extracted from the interpretation of a proxy.

Sediments accumulated in deep areas of Bransfield subbasins have been described as opaline silica-rich muds and sandy muds with variable amounts of volcanic ash (Holler, 1989; Jeffers and Anderson, 1990; Yoon *et al.*, 1994; Banfield and Anderson, 1995).

Bárcena *et al.* (1998) already published a first study on the micropalaeontogical content of GEBRA-1 and GEBRA-2 sediments and its palaeoclimatic and palaeoceanographic significance. In the present study we focus on the sedimentary processes responsible for the accumulation of fine-grained sediments in the Bransfield Basin (BB) and on the likely regional and global sig-

* Corresponding author.

 0959-6836(00)HL431RP

nificance of the climatic record for the last 2850 years as depicted from sediment geochemistry.

Setting

Geodynamic framework and physiography

The Bransfield Strait (BS) is located between the South Shetland Islands (SSI) and the northeastern tip of the AP (61–64°S). The underwater expression of the BS is the BB, a narrow, volcanic and seismically active extensional basin (Gràcia *et al.*, 1997) (Figure 1). The NE–SW oriented BB is divided into three subbasins: Western, Central and Eastern. The Western Basin is the shallowest basin and is flanked by shelves 20–50 km wide. The Central Bransfield Basin (CBB) has a relatively wide continental margin (almost 100 km) on the AP side characterized by a ≈50 km wide shelf and a sinuous, staircase-like slope, while the South Shetland Islands' margin has a narrow shelf (<20 km) and a steep slope (Prieto *et al.*, 1997). The basin floor increases gradually its depth to the NE up to almost 2000 m. It is longitudinally divided by a NE–SW discontinuous volcanic axis. The Eastern Bransfield Basin (EBB) is deeper than the CBB (2750 m) and has relatively wide margins (50–125 km) at both sides with 40–80 km wide shelves and sinuous slopes. The basin floor is divided in lozenge-shaped depressions separated by structural volcanic highs (Gràcia *et al.*, 1996).

Physical oceanography

The BB is strongly influenced both by waters from the Weddell Sea and the Scotia Sea (Paterson and Sievers, 1980). Because of its location in the Southern Ocean, three distinct water masses are identified in the BB (Calafat *et al.*, 1997). The warm and low salinity Transitional Bellinghausen Water (TBW) (2.25°C and 33.50 psu) and the cold and salty Transitional Weddell Water (TWW) (0.75°C and 34.40 psu) occupy the 300 upper metres. The isotherm of the 1°C and the isohaline of 34.1 psu have been suggested as the limit between these two water masses. The 34.5 psu isohaline that lies at around 300 m depth defines the upper limit of the Bransfield Deep Water (BDW) (typically >1°C and 34.53 psu), which may have influences from three different sources: the Circumpolar Deep Water (CDW), entering the BB by its southwestern end; waters belonging to the Weddell Sea sequence; and dense shelf waters coming from the eastern AP continental shelf as depth and density increase (Whitworth *et al.*, 1994).

The surface circulation in the BB is characterized by the northeast geostrophic flow of TBW in the proximity of SSI, and by the southwestward geostrophic flow of TWW on the AP side. A sharp superficial geostrophic front is identified approximately over the axis of the CBB at the limit between the two water masses (Niiler *et al.*, 1991; García *et al.*, 1994). Two additional subsurface fronts located over the SSI and the AP slopes in the CBB affect intermediate waters and define the extent of the local shelf waters and the inflow of the Weddell Sea system waters (García *et al.*, 1994). Deep circulation is mainly linked to the entrance of dense Weddell shelf waters through the Antarctic Sound and around the NE tip of Joinville Island (Whitworth *et al.*, 1994; López *et al.*, 1999) and their sinking over the shelf and the slope.

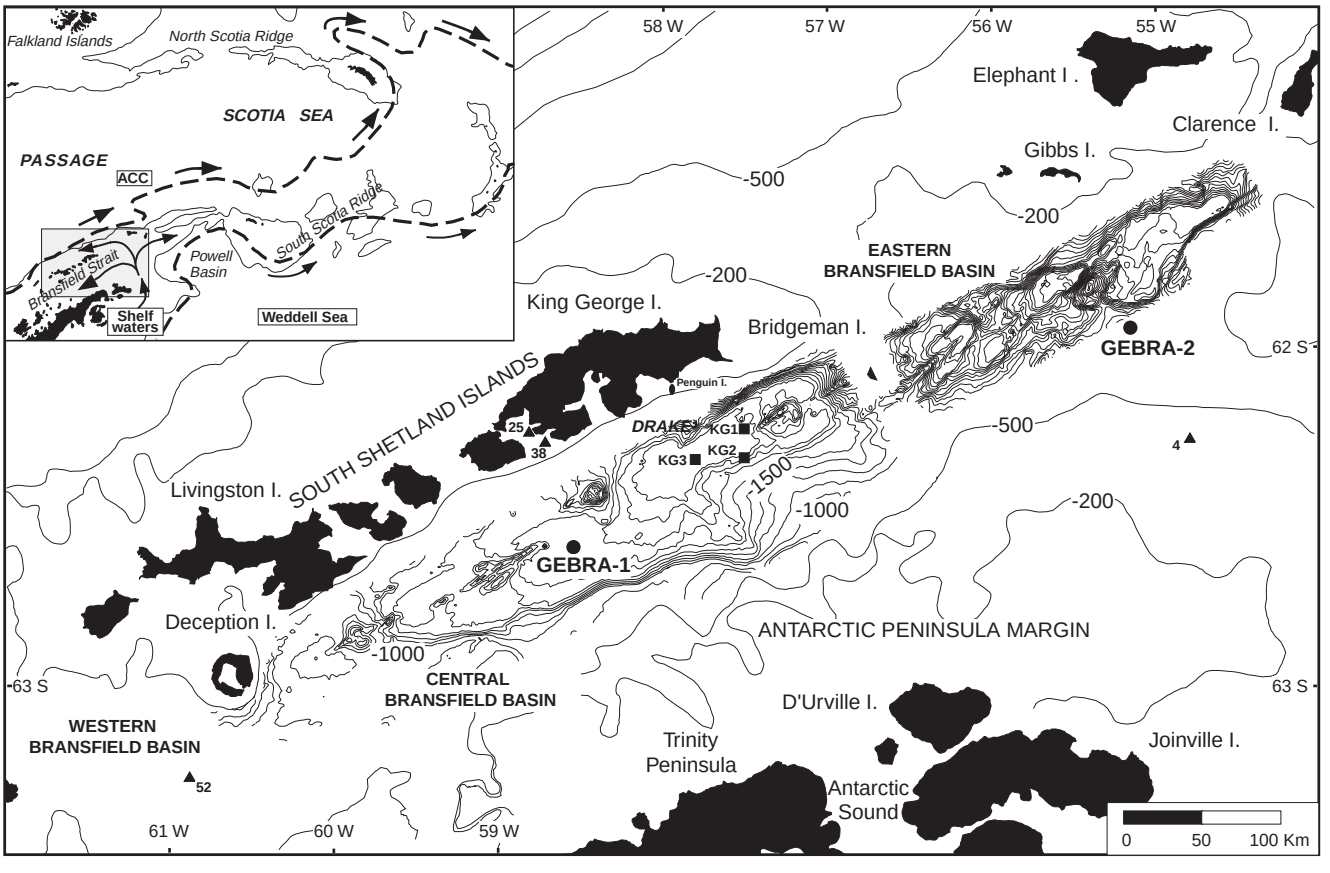

Figure 1 Bathymetric map of Bransfield Basin (Gràcia *et al.*, 1996) with the location of the cores GEBRA-1 and GEBRA-2. The location of sediment traps KG1-KG3 (Wefer *et al.*, 1988; 1990) and the shelf sediment samples (G8601-4, G8601-25, G8601-38 and G8601-52) (DeMaster *et al.*, 1987) used for comparison is also shown. Thin lines in the Central and Eastern Bransfield Basin are 100 m isobaths. The sketch map in the upper left corner shows the domains of the principal water mass sequences in the region and their flow paths (indicated by arrows) (Whitworth *et al.*, 1994). The heavy dashed lines show the southern extent of Antarctic Contour Current (ACC) sequence waters and the northern extent of Weddell Sea sequence waters.

Present climatic conditions, glacial setting and sea-ice distribution

The AP is under the mildest climatic conditions of the whole southern continent and acts as a topographic barrier between pseudocontinental conditions on its Weddell side and maritime conditions on its Pacific side. The maritime climate is characterized by high wetness and mean annual, summer and winter temperatures higher than –4°C, 0°C (≈2°C in the SSI) and –10°C, respectively. Areas surrounding BS experience annual solid and liquid average precipitation above 1000 mm (Griffith and Anderson, 1989). Late-summer snow-line in SSI is located around 150 m (Domack and Ishman, 1993) leading to abundant meltwater during this period. Such climatic conditions control the distribution, type and glacial regime of the glaciers that flow to BB. Glaciers in SSI and Trinity Peninsula belong to relatively thin ice fields that extend discontinuously to the coast in form of piedmont and valley glaciers. In SSI, this results in a setting in which less than half the coastline is occupied by tidewater glaciers grounded at an average of 80 to 120 m depth. The rest of the coastline is bare rock or wide gravel beaches, some of which are occupied by valley glaciers on their onshore end. These glaciers frequently present turbid proglacial streams during summer period (Yoon *et al.*, 1997; 1998). Climatic conditions also control the permanence and distribution of winter sea ice in BB, which is normally ice-free between December and April. During May and June sea ice starts growing first along the AP margin and by July it has spread to the north covering the whole strait. The area remains totally ice-covered for approximately four months until mid-October when the sea ice starts opening (Griffith and Anderson, 1989). By contrast with other areas in the Southern Ocean, the sea-ice advance is a relatively brief event (a few weeks) while the sea-ice retreat is gradual (several months) (Leventer *et al.*, 1996).

Materials and methods

During the GEBRA '93 cruise on board the Spanish R.V. *Hespérides*, two gravity cores (GEBRA-1 and GEBRA-2) were obtained in the Central and Eastern Bransfield basins (Canals and GEBRA'93 Team, 1993). Core GEBRA-1 is 252 cm long and was obtained in a flat area (62°35.36′S/58°32.53′W, 1652 m depth) over the axis of the CBB between two volcanic edifices (Figure 1). The seismic facies on the core location are dominantly stratified, with some lenses of chaotic and transparent facies at the bottom of small depressions (for detailed Bottom Parametric Source, BPS, and seismic profiles near the core locations, see Bárcena *et al.*, 1998, and Prieto *et al.*, 1999). Core GEBRA-2 is 444 cm long and was obtained on top of a prominent sediment mound over the AP slope of the EBB (61°56.56′S/55°20.21′W, 1106 m depth). This sediment mound is 300 m high, located downslope of the foot of a 600 m scarp, and the seismic facies are stratified on its northern side, where GEBRA-2 was obtained, and chaotic and transparent on its southern side.

Each of the cores was opened and visually described on board and, once in the laboratory, they were systematically subsampled (1 cm thick samples) at 5 cm intervals for sedimentological (grain size and physical properties), mineralogical and geochemical analyses (C, N, biogenic silica). Grain-size analysis was done through 63 μm wet sieving of hydrogen peroxide treated samples. The mud fraction finer than 63 μm was afterwards analysed using a laser particle sizer COULTER-LS, with a resolution of 100 channels between 0.4 and 1000 μm. Weight percentages of sand (>63 μm), silt (63–4 μm) and clay (<4 μm) were recalculated and normalized to 100%. Mean mud size was also used for a better resolution of grain-size fluctuations. Mean mud size (X_a) is the average size of all the particles in one sample and is calculated from the expression $X_a = \Sigma\ (X_c \cdot n_c)/\Sigma n_c$, where X_c is the median size of the channel in μm and n_c is the percentage of particles in each channel. Physical properties were calculated following the gravimetrical procedures described by Boyce (1976). The mineralogical composition was determined on normal and ethylene-glycol treated oriented aggregates of particles smaller than 4 μm. The analyses were done using a Siemens D-500 diffractometer with a Cu anode (1.5418 Å, 40 kV and 30 mA), a reception window of 0.05° and a scanning speed of de 1°2 $\theta \cdot \text{min}^{-1}$. Once main mineralogical phases were identified, the semiquantitative method of Biscaye (1965) was applied in order to assess downcore mineralogical variations. Organic carbon and nitrogen content were determined using 1M HCl decalcified samples in an elemental analyser Fisons 1500. Biogenic silica content was measured through Mortlock and Froelich (1989) wet alkaline leaching (2N Na_2CO_3) and the resultant solutions were analysed with Inductive Coupled Plasma Atomic Emission Spectrosmetry (ICP-AES). Si weight concentrations were transformed into biogenic opal concentrations multiplying the obtained values by a factor of 2.4 (Mortlock and Froelich, 1989). Moreover, organic carbon of three samples per core (top, middle and base of the core), taken just after core opening and kept frozen, were AMS ^{14}C dated in the R.J. Van der Graaf Laboratorium of Utrecht (Van der Borg *et al.*, 1987). Additionally, ^{210}Pb and ^{137}Cs were determined in the topmost 10 cm of each core by γ-spectrometry in an n-type high-purity germanium detector.

Table 1 ^{14}C ages and δ^{13}C of the AMS analysed samples of cores GEBRA-1 and GEBRA-2

Core	Depth (cm)	Laboratory code	Measured age (^{14}C yr BP)	$\delta\ ^{13}$C (‰)
GEBRA-1	28–29	UtC-5310	2985 ± 39 BP	–23.7
	135–136	UtC-5311	3959 ± 47 BP	–24.6
	240–241	UtC-5312	4646 ± 37 BP	–25.2
GEBRA-2	25–26	UtC-5313	2796 ± 34 BP	–25.3
	225–226	UtC-5314	3916 ± 36 BP	–25.5
	440–441	UtC-5315	5385 ± 39 BP	–26.1

Results

Chronology

^{14}C analyses of the three samples of each core give the values of ^{14}C ages and δ^{13}C displayed in Table 1. Linear regression applied to ^{14}C ages results in sedimentation rates of 0.128 ± 0.010 $\text{cm} \cdot \text{yr}^{-1}$ for GEBRA-1 and 0.161 ± 0.009 $\text{cm} \cdot \text{yr}^{-1}$ for GEBRA-2. Surface ages obtained by extrapolation of the regression lines up to 0 cm depth are 2797 ± 106 and 2598 ± 97 years for GEBRA-1 and GEBRA-2, respectively. Consideration of dating method error ranges for calculating sedimentation rates and surface ages results in small differences with the data formerly published by Bárcena *et al.* (1998). Our sedimentation rates and surface ages are comparable as well with the values obtained by Harden *et al.* (1992) in the same area. Regarding these sedimentation rates, the 1 cm thick samples taken at 5 cm intervals in each core represent *c.* eight and *c.* six years each, and are spaced *c.* 40 and *c.* 30 years for GEBRA-1 and GEBRA-2 respectively.

Analyses of ^{210}Pb in core tops show an excess of ^{210}Pb activity (65 ± 14 $\text{Bq} \cdot \text{kg}^{-1}$) in GEBRA-1 while not excess ^{210}Pb was detected in GEBRA-2 (Bárcena *et al.*, 1998). No ^{137}Cs signal in any of both core tops was observed. Implications of all the chronology data will be further discussed in the age model section below.

Lithological description

Materials recovered in Central and Eastern Bransfield basins are mainly clayey silts. Sediments have an overall olive colour ranging from olive grey colour (7.5 Y) to dark olive green colour (10 Y), except the two topmost centimetres of GEBRA-1 that have a brownish green colour (2.5 Y). The clayey silts show different degrees of centimetric to millimetric parallel lamination, made by an alternation of dark and light millimetric to centimetric lamina. The limits between different facies are transitional and no sharp contacts were observed. Five clayey silt facies are identified in both cores regarding lamination: massive silts (Sm), diffusely laminated silts with centrimetric lamination (Sd), centimetrically laminated silts (SI), millimetrically laminated silts (SII) and dark silt layers (Sb) (Figure 2). A sixth sandy silt facies (Ss), rich in volcanic ashes, is recognized between 245 cm depth and the core base in GEBRA-1 and between 302 and 306.5 cm depth in GEBRA-2.

Sediment grain size and dry density

The silty character of the sediments is confirmed by the data of grain-size analyses (Tables 2 and 3). Sediments from CBB floor (core GEBRA-1) are slightly finer than those on the AP slope of the EBB (core GEBRA-2) that have higher sand and silt contents. The percentage of each fraction is almost constant along each of the cores (Tables 2 and 3; Figures 3 and 4) except some 'coarse layers' in which the sand content increases remarkably above the average. Coarse layers are found at the base (247 cm) and at the top (between 0 and 40 cm) of core GEBRA-1 (Figure 3) and randomly distributed in GEBRA-2 from 100 cm to the core base. The higher number of coarse layers by thickness unit causes the coarser character of the GEBRA-2 sediments (Figure 4). The sand fraction of the coarse layers identified in GEBRA-1 is composed mainly of volcanic ashes, while diatom frustules, sponge spicules and quartz grains predominate in the sand fraction of coarse layers of core GEBRA-2.

A distinct peak in mean mud size coinciding with a peak in sand content (16.5% sand) is identified between the base and 246 cm depth of core GEBRA-1. The section between 246 cm and the core top is characterized by a series of mean mud-size oscillations of low frequency and amplitude (Figure 3). Core GEBRA-2 shows high-frequency mean mud-size oscillations, especially below 125 cm depth (Figure 4), coinciding with the section in which coarse layers are found. It is important to notice that only in the section between the base and 246 cm depth values of mean size of mud particles are above 30 μm, denoting the exceptional coarse character of this layer.

The sediments in both cores have low dry densities. A relation between sand content and physical properties is suggested by higher dry density values on some of the layers richer in sand, particularly in core GEBRA-1 (Figures 3 and 4). The grain-size peak identified at the base of GEBRA-1 is also reflected by the dry density log (Figure 3). Furthermore, a gentle increase in dry density with depth is displayed along core GEBRA-2 (Figure 4).

Mineralogy

The three main minerals identified in the clay fraction are chlorite, smectite and illite. In some of the samples, small amounts of kaolinite and other accessory minerals such as quartz, feldspars (sodian anortite), pyroxenes and opal are also present.

Chlorite diffraction pattern shows an intense peak at 14.2 Å, a very intense peak at 7.12 Å, a weak peak at 4.75 Å, and again a very intense peak at 3.54 Å. This sequence is typical of iron rich chlorites (Grim, 1953). The method used for mineralogical analyses does not allow exact determination of the contribution of kaolinite to the diffraction peaks of chlorite when the amount of kaolinite is relatively small compared to the amount of chlorite. Only a small peak at 3.58 Å can be identified in some samples. Yoon

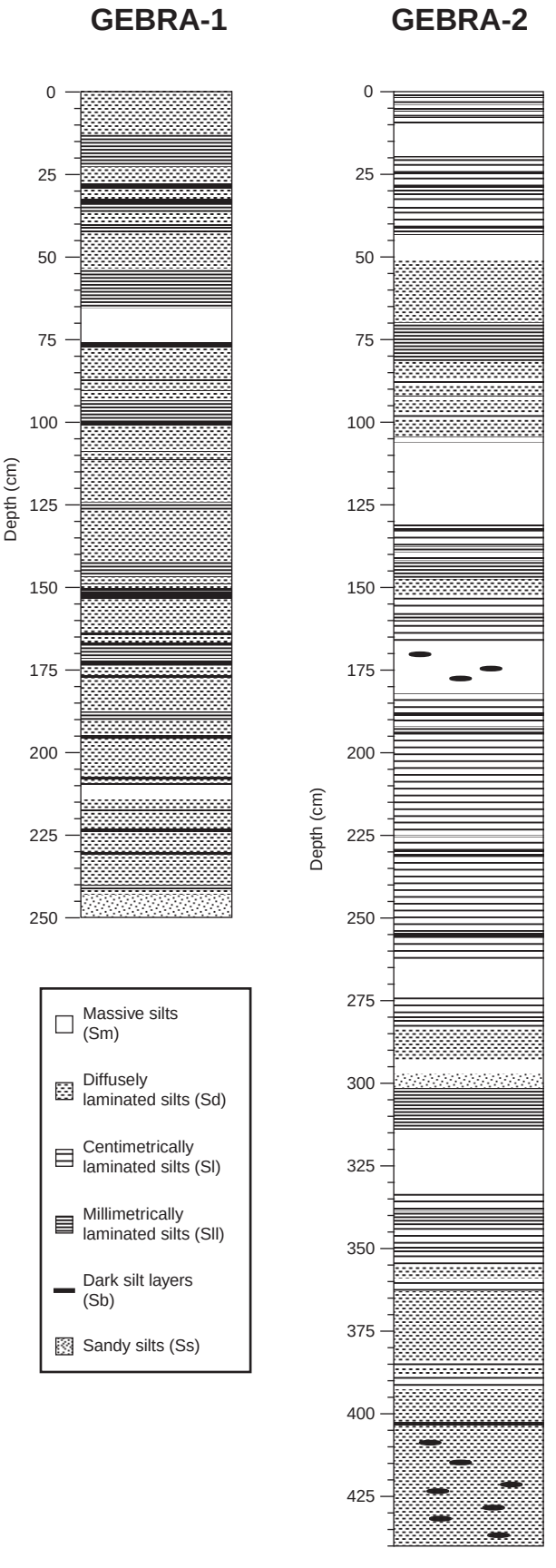

Figure 2 Detailed lithological logs of cores GEBRA-1 and GEBRA-2.

et al. (1992) found kaolinite contents around 5% and less than 5% in surface sediments from the areas where cores GEBRA-1 and GEBRA-2 were retrieved, respectively. Thus, chlorite and kaolinite are considered together in the semiquantitative analyses. The term 'smectite' is used to designate those expandable clay minerals that give a broad peak in the region of 12.8 Å in normal

Table 2 Sedimentological, mass-physical, mineralogical and geochemical data from core GEBRA-1 (Smc. Smectite, Ill. Illite, Chl. Chlorite, Kaol. Kaolinite)

Depth (cm)	Sand (%)	Silt (%)	Clay (%)	Mean mud size (μm)	Dry density (g/cm^3)	Smc. (%)	Ill. (%)	Chl. (+Kaol) (%)	Org. C (%)	N (%)	C/N	Opal (%)
0.5	6.69	71.80	21.51	14.76	0.37	8.82	32.50	58.68	1.14	0.16	6.97	12.20
5.5	2.43	68.14	29.43	11.83	0.42	15.44	23.16	61.40	1.13	0.17	6.73	14.85
10.5	6.70	65.18	28.12	11.57	0.47	10.18	29.84	59.98	0.99	0.15	6.52	14.55
15.5	2.90	70.28	26.82	12.98	0.43	20.02	22.46	57.53	1.17	0.18	6.62	14.39
20.5	1.77	73.78	24.45	12.14	0.47	23.53	21.41	55.07	1.21	0.20	6.03	17.29
25.5	6.01	69.64	24.35	12.18	0.67	23.66	26.14	50.20	1.20	0.17	6.99	17.80
28.5	2.09	82.19	15.72	14.52	0.29	5.50	22.71	71.78	1.46	0.24	6.20	22.93
30.5	1.65	73.60	24.74	13.74	0.35	22.16	22.21	55.63	1.30	0.21	6.36	19.48
35.5	10.62	68.14	21.24	12.77	0.49	9.32	17.25	73.43	1.00	0.16	6.43	16.54
40.5	2.15	70.54	27.31	12.20	0.52	21.76	21.74	56.50	1.17	0.19	6.08	16.83
45.5	1.41	70.03	28.56	13.90	0.44	12.98	25.42	61.60	1.19	0.18	6.60	18.98
50.5	1.23	75.19	23.58	13.40	0.33	18.43	30.07	51.50	1.45	0.21	6.92	22.00
55.5	1.81	72.67	25.52	13.27	0.40	15.81	24.67	59.52	1.39	0.22	6.36	19.69
60.5	2.50	67.75	29.75	11.03	0.42	21.63	21.99	56.38	1.26	0.22	5.80	17.19
65.5	1.67	69.32	29.01	11.45	0.43	21.96	31.02	47.01	1.18	0.19	6.34	14.00
70.5	1.29	68.56	30.15	10.67	0.47	16.01	29.14	54.85	1.20	0.18	6.59	11.83
75.5	0.75	71.89	27.36	12.40	0.49	18.77	26.57	54.65	1.38	0.22	6.20	17.27
80.5	1.57	73.22	25.22	12.72	0.38	18.43	22.06	59.51	1.43	0.18	7.73	17.10
85.5	2.87	73.47	23.66	12.72	0.34	7.90	24.04	68.06	1.35	0.22	6.10	16.47
90.5	1.58	75.24	23.18	15.22	0.42	14.65	20.13	65.21	1.48	0.22	6.84	15.56
95.5	1.61	72.92	25.47	13.22	0.33	13.74	22.65	63.60	–	–	–	19.36
100.5	1.89	69.71	28.40	11.91	0.36	5.32	25.07	69.61	1.43	0.23	6.28	16.73
105.5	1.38	71.54	27.08	12.67	0.33	17.01	29.80	53.19	1.35	0.21	6.59	13.24
110.5	1.99	68.30	29.71	12.84	0.35	22.84	24.86	52.30	1.19	0.18	6.69	17.03
115.5	1.28	71.78	26.94	12.01	0.48	0.00	28.80	71.20	0.97	0.16	6.17	14.13
120.5	2.30	69.69	28.01	13.13	0.38	13.71	28.30	57.99	1.29	0.19	6.93	18.01
125.5	0.87	68.68	30.46	13.24	0.36	–	–	–	1.17	0.19	6.03	17.65
130.5	2.44	70.21	27.36	12.31	0.43	13.83	34.64	51.54	1.10	0.16	6.85	14.29
135.5	1.55	70.09	28.36	11.77	0.43	7.93	36.15	55.92	1.21	0.18	6.84	16.62
140.5	1.32	68.77	29.91	11.42	0.43	12.35	25.91	61.74	1.22	0.20	6.18	17.82
145.5	1.55	70.66	27.79	11.50	0.42	11.15	28.42	60.43	1.25	0.20	6.17	21.59
150.5	1.85	68.27	29.88	11.17	0.42	8.67	29.69	61.65	1.23	0.18	6.85	17.23
155.5	3.65	71.34	25.01	12.97	0.46	14.29	28.63	57.09	1.20	0.19	6.29	18.49
160.5	2.06	72.29	25.65	13.24	0.49	23.18	23.82	53.00	1.15	0.19	6.12	18.14
165.5	1.96	74.34	23.70	11.62	0.46	23.20	22.68	54.12	1.25	0.19	6.54	19.76
170.5	0.78	72.96	26.26	12.60	0.42	5.36	23.08	71.56	1.28	0.19	6.63	18.96
175.5	2.98	69.30	27.71	11.35	0.45	12.82	49.61	37.57	1.16	0.17	6.65	17.63
180.5	0.85	71.67	27.49	11.26	0.28	27.49	27.49	45.02	1.18	0.20	5.83	16.19
185.5	1.99	72.67	25.34	11.83	0.58	29.21	23.48	47.32	1.27	0.18	6.90	20.12
190.5	1.53	73.70	24.77	13.90	0.42	35.14	32.14	32.72	1.16	0.19	6.12	17.94
195.5	0.92	78.43	20.65	15.52	0.43	26.33	20.28	53.39	1.36	0.20	6.75	20.50
196.5	4.25	82.23	13.52	14.97	0.38	9.50	28.27	62.23	1.46	0.23	6.29	24.11
200.5	1.35	67.58	31.07	10.88	0.58	30.31	24.36	45.32	1.04	0.15	6.94	14.90
205.5	1.19	68.78	30.03	11.16	0.64	30.79	22.10	47.12	1.09	0.17	6.30	14.46
210.5	1.61	74.54	23.84	12.08	0.68	31.73	22.98	45.29	1.10	0.18	6.06	15.50
215.5	1.25	72.34	26.41	13.01	0.48	20.85	29.02	50.13	1.31	0.19	6.98	17.38
220.5	1.02	73.16	25.82	12.62	0.51	24.55	29.44	46.01	1.14	0.17	6.65	18.69
225.5	1.75	75.07	23.18	13.71	0.62	31.64	20.12	48.24	0.91	0.14	6.49	12.71
230.5	2.19	71.18	26.63	12.66	0.49	28.76	29.14	42.10	1.17	0.20	5.81	15.45
235.5	2.43	69.94	27.64	11.57	0.55	37.14	18.88	43.98	1.03	0.16	6.56	14.16
240.5	1.58	71.97	26.46	11.77	0.61	5.90	33.68	60.42	1.23	0.18	6.81	17.25
245.5	0.62	73.03	26.35	12.07	0.65	38.41	19.09	42.51	1.08	0.17	6.41	15.30
247.5	16.45	77.20	6.35	35.06	1.30	26.66	20.17	53.16	0.26	0.00	0.00	4.69
250.5	4.38	74.13	21.49	15.79	1.05	29.75	25.58	44.67	0.72	0.11	6.29	10.70
Mean	2.53	71.83	25.64	13.04	0.48	18.80	26.09	55.11	1.19	0.18	6.49	16.73

aggregates, which shifts to 16.9 Å in the glycol-treated aggregates. Illite is easily identified by the presence of the peak sequence at 10, 5 and 3.34 Å.

Tables 2 and 3 display the contents of the three main mineral phases in the BB cores. Considering that kaolinite has a very small contribution, chlorite is the most abundant mineral in the clay fraction of both cores. In GEBRA-1 core illite is more abundant than smectite whereas in GEBRA-2 core illite and smectite mean contents are very close. The in-depth evolution of the mineralogical composition is controlled in both cores by changes in the relative abundances of chlorite and smectite since fluctuations in illite content are quite small compared to

Table 3 Sedimentological, mass-physical, mineralogical and geochemical data from core GEBRA-2 (Smc. Smectite, Ill. Illite, Chl. Chlorite, Kaol. Kaolinite)

Depth (cm)	Sand (%)	Silt (%)	Clay (%)	Mean mud size (μm)	Dry density (g/cm^3)	Smc. (%)	Ill. (%)	Chl. (+Kaol) (%)	Org. C (%)	N (%)	C/N	Opal (%)
0.5	3.52	78.94	17.54	16.58	0.57	13.45	14.69	71.86	1.11	0.17	6.40	17.58
5.5	2.99	75.38	21.63	15.99	0.52	11.18	22.95	65.87	1.13	0.19	6.12	21.49
10.5	3.32	74.99	21.69	15.76	0.48	7.48	24.85	67.67	1.14	0.18	6.34	20.21
15.5	3.62	77.49	18.89	17.13	0.61	16.91	19.92	63.17	1.08	0.16	6.69	18.61
20.5	3.32	75.91	20.78	15.96	0.62	21.26	24.87	53.86	1.12	0.18	6.17	19.97
25.5	2.37	77.79	19.84	16.17	0.42	10.55	18.83	70.62	1.16	0.20	5.77	23.81
30.5	3.77	79.55	16.67	17.39	0.48	22.97	22.78	54.25	1.21	0.21	5.81	23.81
35.5	2.88	81.06	16.07	16.00	0.45	16.46	17.10	66.44	1.25	0.21	5.84	25.32
40.5	3.07	78.84	18.09	16.05	0.50	19.63	16.94	63.43	1.20	0.20	5.96	24.59
45.5	3.61	74.82	21.56	14.88	0.52	19.46	21.63	58.90	1.13	0.17	6.64	19.68
50.5	2.27	74.18	23.55	14.88	0.53	29.70	25.42	44.88	1.11	0.18	6.15	20.99
55.5	2.37	75.70	21.93	13.98	0.45	12.21	28.68	59.11	1.41	0.22	6.35	22.59
60.5	2.44	73.13	24.43	14.25	0.55	29.77	21.14	49.09	1.27	0.20	6.34	19.61
65.5	2.88	75.91	21.21	15.17	0.59	20.14	23.65	56.20	1.06	0.17	6.31	18.28
70.5	2.61	73.37	24.02	14.94	0.48	25.02	20.63	54.36	1.15	0.17	6.72	19.54
75.5	3.09	79.06	17.85	15.14	0.42	31.95	24.05	44.00	1.30	0.20	6.51	23.33
80.5	3.38	73.02	23.60	14.33	0.50	30.62	23.04	46.35	1.37	0.22	6.17	24.25
85.5	3.27	73.18	23.55	12.92	0.46	37.05	21.40	41.55	1.29	0.21	6.05	23.93
90.5	2.74	78.43	18.83	15.95	0.55	28.14	21.20	50.67	1.23	0.21	5.84	22.88
95.5	2.61	78.00	19.39	15.16	0.49	33.25	27.31	39.45	1.18	0.19	6.19	21.79
100.5	5.69	75.42	18.89	16.43	0.46	26.18	28.21	45.61	1.17	0.19	6.19	20.32
105.5	5.91	74.41	19.67	14.88	0.57	24.03	24.16	51.81	1.13	0.18	6.13	22.56
110.5	3.99	70.87	25.14	13.28	0.49	31.35	25.76	42.89	1.13	0.17	6.57	24.11
115.5	4.86	75.84	19.30	14.89	0.59	18.01	24.46	57.53	1.10	0.17	6.46	21.55
120.5	3.77	73.29	22.94	14.47	0.57	27.16	26.47	46.37	1.13	0.19	5.98	20.59
125.5	2.75	74.70	22.55	14.36	0.57	20.20	26.17	53.64	1.12	0.17	6.76	19.76
130.5	8.34	69.90	21.76	14.06	0.55	27.41	24.14	48.45	1.12	0.18	6.38	21.43
135.5	4.32	73.04	22.64	14.64	0.57	21.85	25.67	52.48	1.35	0.22	6.23	21.98
140.5	5.14	75.78	19.08	16.84	0.59	27.72	23.82	48.45	1.11	0.18	6.05	20.96
145.5	4.78	75.83	19.39	15.23	0.49	19.17	22.76	58.07	1.11	0.18	6.07	20.51
150.5	12.53	73.11	14.35	18.54	0.53	30.19	25.09	44.72	1.16	0.20	5.96	20.87
155.5	2.24	74.73	23.03	16.12	0.52	24.34	26.63	49.03	1.24	0.20	6.17	21.36
160.5	3.32	77.38	19.29	16.93	0.49	29.83	23.17	47.00	1.10	0.17	6.41	21.59
165.5	4.40	77.74	17.86	18.69	0.49	30.44	21.84	47.72	1.13	0.18	6.20	22.07
170.5	7.61	75.15	17.24	16.53	0.56	28.64	19.78	51.58	1.07	0.16	6.49	18.54
175.5	5.05	74.72	20.23	15.34	0.56	31.30	25.90	42.80	1.07	0.17	6.16	20.27
180.5	3.28	73.58	23.14	15.40	0.55	30.08	28.18	41.74	1.05	0.18	5.91	20.58
185.5	3.12	77.02	19.86	15.81	0.57	25.57	23.73	50.70	1.09	0.19	5.84	19.41
190.5	3.51	74.96	21.52	15.77	0.59	30.16	25.47	44.37	1.05	0.17	6.24	21.79
195.5	5.18	76.72	18.10	17.06	0.46	16.66	28.67	54.67	1.13	0.19	6.11	24.99
200.5	2.58	73.87	23.55	15.37	0.48	36.13	23.35	40.52	1.11	0.18	6.27	23.57
205.5	3.07	73.14	23.79	13.62	0.49	29.92	25.59	44.49	1.20	0.19	6.39	24.87
210.5	4.07	74.49	21.44	16.70	0.56	31.95	24.37	43.68	1.16	0.18	6.28	22.53
215.5	4.13	73.70	22.17	13.55	0.61	31.00	26.88	42.12	1.15	0.19	6.06	23.51
220.5	2.27	76.49	21.24	17.02	0.52	33.46	25.12	41.42	1.18	0.18	6.61	24.23
225.5	2.53	76.52	20.96	17.19	0.49	33.22	27.52	39.26	1.18	0.19	6.12	24.06
230.5	4.70	74.47	20.83	16.36	0.53	34.12	25.02	40.87	1.15	0.17	6.73	23.81
235.5	6.70	75.74	17.56	15.99	0.52	15.05	31.40	53.55	1.20	0.19	6.31	23.68
240.5	3.71	78.74	17.55	17.34	0.51	32.54	25.26	42.20	1.20	0.20	6.04	22.56
245.5	5.20	79.44	15.36	17.01	0.48	19.28	23.11	57.61	1.25	0.21	5.99	23.18
250.5	2.74	74.29	22.96	19.89	0.53	29.62	26.71	43.67	1.18	0.19	6.23	22.96
255.5	10.75	72.30	16.95	15.66	0.50	26.21	30.63	43.16	1.15	0.19	6.20	22.44
260.5	3.53	74.91	21.56	16.78	0.54	34.97	23.72	41.31	1.10	0.18	6.14	23.58
265.5	6.54	75.99	17.47	17.50	0.54	24.07	28.01	47.92	1.21	0.19	6.30	21.68
270.5	7.95	74.07	17.98	14.61	0.45	17.45	19.60	62.96	1.13	0.19	6.08	25.36
275.5	5.19	80.18	14.63	16.68	0.51	17.70	24.67	57.63	1.16	0.19	6.17	22.49
280.5	12.13	71.25	16.62	14.25	0.45	12.50	22.60	64.91	1.15	0.19	6.08	24.32
285.5	2.57	73.09	24.34	14.86	0.57	39.57	23.71	36.73	1.07	0.17	6.17	18.84
290.5	20.14	69.18	10.68	20.45	0.58	12.55	20.93	66.52	1.14	0.18	6.29	22.45
295.5	5.72	70.14	24.13	13.13	0.60	46.84	20.21	32.94	1.16	0.20	5.76	23.49
300.5	6.26	74.93	18.80	18.92	0.68	41.14	20.82	38.04	0.85	0.15	5.77	19.28
305.5	16.50	67.44	16.06	16.64	0.50	19.90	24.74	55.36	1.14	0.18	6.42	22.93
310.5	6.10	76.28	17.61	16.36	0.50	15.39	23.02	61.59	1.21	0.20	6.09	25.09
315.5	4.99	75.79	19.22	16.99	0.53	16.46	27.33	56.21	1.24	0.19	6.42	26.43

Table 3 Continued

Depth (cm)	Sand (%)	Silt (%)	Clay (%)	Mean mud size (μm)	Dry density (g/cm^3)	Smc. (%)	Ill. (%)	Chl. (+Kaol) (%)	Org. C (%)	N (%)	C/N	Opal (%)
320.5	1.27	77.56	21.18	18.74	0.56	36.80	21.96	41.24	1.17	0.19	6.29	24.69
325.5	3.62	75.10	21.28	16.69	0.50	31.32	25.67	43.01	1.18	0.20	5.84	25.67
330.5	2.29	76.18	21.53	18.87	0.58	37.35	23.13	39.52	0.98	0.16	6.30	21.69
335.5	5.12	74.29	20.59	17.24	0.46	30.96	22.38	46.66	1.16	0.20	5.68	27.58
340.5	8.48	77.03	14.49	18.28	0.54	18.44	28.55	53.02	1.13	0.19	5.85	24.29
345.5	9.30	75.61	15.09	18.12	0.51	12.32	24.40	63.27	1.18	0.20	5.76	25.09
350.5	5.12	77.12	17.76	16.88	0.56	37.56	23.84	38.60	1.10	0.19	5.92	22.42
355.5	5.67	75.81	18.52	16.59	0.47	23.93	24.66	51.41	1.16	0.19	6.00	25.87
360.5	4.59	79.57	15.83	18.55	0.57	26.36	27.64	46.00	1.11	0.19	5.73	23.43
365.5	4.61	78.74	16.65	18.77	0.53	20.00	28.53	51.47	1.17	0.21	5.48	
370.5	6.21	74.00	19.79	15.81	0.58	25.96	28.92	45.11	1.03	0.17	6.05	22.60
375.5	6.86	75.41	17.73	17.24	0.57	18.88	27.38	53.75	1.16	0.19	6.13	22.75
380.5	7.48	74.70	17.82	19.36	0.53	15.87	25.13	59.00	1.22	0.22	5.61	25.64
385.5	6.17	72.18	21.66	16.30	0.51	19.93	26.78	53.29	1.14	0.19	5.89	22.42
390.5	7.77	74.93	17.30	17.08	0.47	20.92	26.39	52.69	1.29	0.21	6.09	25.06
395.5	6.09	77.42	16.50	18.22	0.57	35.56	26.05	38.40	1.13	0.21	5.37	24.45
400.5	8.17	74.95	16.88	15.97	0.58	7.78	29.41	62.81	1.09	0.19	5.61	24.60
405.5	5.28	76.77	17.96	17.66	0.58	17.20	29.65	53.16	1.10	0.18	6.18	24.76
410.5	3.69	78.65	17.66	18.86	0.60	27.17	26.05	46.78	1.12	0.18	6.33	25.71
415.5	4.53	74.93	20.55	15.96	0.62	39.52	22.57	37.91	1.12	0.19	5.92	23.07
420.5	6.13	70.59	23.28	16.25	0.64	19.71	24.46	55.84	1.15	0.18	6.24	22.28
425.5	3.56	70.83	25.60	15.20	0.60	24.00	23.58	52.42	1.13	0.17	6.61	23.29
430.5	5.02	72.63	22.35	17.60	0.62	11.47	25.48	63.05	1.14	0.19	6.12	23.23
435.5	6.46	74.37	19.17	17.94	0.59	32.05	27.35	40.60	1.18	0.20	5.78	23.70
440.5	4.01	73.41	22.58	17.30	0.62	37.81	22.90	39.28	1.16	0.20	5.85	21.82
443.5	7.96	74.03	18.01	15.63	0.62	37.61	24.89	37.50	1.08	0.19	5.79	22.96
Mean	5.06	75.18	19.76	16.31	0.54	25.28	24.48	50.24	1.15	0.19	6.13	22.63

the fluctuations of the other two main minerals (Tables 2 and 3; Figures 3 and 4). GEBRA-1 log is characterized by low frequency and high-amplitude oscillations while the opposite is observed in GEBRA-2 log, which shows high frequency and low-amplitude oscillations.

Geochemistry (C, N and opal)

The abundances of organic carbon, nitrogen and opal at each depth are displayed in Tables 2 and 3. Mean carbon and nitrogen percentages are very similar in both cores (1.19% and 0.18% and 1.15% and 0.19% for GEBRA-1 and GEBRA-2, respectively). The C/N index fluctuates between 5.80 and 7.73, with a mean value of 6.49 in GEBRA-1, and between 5.73 and 6.76, with a mean value of 6.13 in GEBRA-2. The largest gross difference in geochemical composition between the two cores is that of the mean opal content which is higher in GEBRA-2 (22.63%) than in GEBRA-1 (16.73%). The square correlation factors (r^2) between organic carbon content and nitrogen and opal contents in core GEBRA-1 are 0.88 and 0.57, respectively. This correlation is obvious from comparing the shape of the three logs (Figure 3). The overall square correlation factor between organic carbon content and nitrogen and opal contents are lower in GEBRA-2 (0.66 and 0.14, respectively) because as seen in Figure 4, below the first metre, the evolution of the content of nitrogen and especially opal show slight differences with respect to the evolution of carbon content.

The most outstanding feature recognized in grain size and dry density logs at the base of core GEBRA-1 is also recognized in geochemical logs (Figure 3), where it appears as a pronounced minimum in biogenic components between the base of the core and 246 cm depth. In the upper section the biogenic logs are characterized by a series of centimetric fluctuations of some percentage tenths for organic carbon, some hundredths for nitrogen and some units for opal. These fluctuations have a cyclical appearance between 125 cm depth and the core top. Organic carbon and nitrogen logs of core GEBRA-2 (Figure 4) show, between the base and 100 cm depth, oscillations of higher frequency but lower amplitude than those observed in the upper section of GEBRA-1. The top section (100 cm depth to core top) presents in contrast a pattern similar to the one observed in the top section of GEBRA-1. Opal log presents an overall decreasing pattern from bottom to top. This decreasing pattern is concentrated around 200 and 300 cm depth where sharp decreases in opal can be observed. Besides those sharp decreases in opal, a similar oscillation pattern to that observed in carbon and nitrogen logs can be identified.

Discussion

Age model

Before establishing the age model for the recovered sediments, we have to determine the origin of the organic matter used for sediment dating. Organic matter accumulated in deep BB sediments is very probably derived from primary producers (phytoplankton) as shown by: (a) the very close values of C/N indexes in the sediment (6.5 ± 0.4 for GEBRA-1 and 6.1 ± 0.3 for GEBRA-2) and in the surface waters (6.4 ± 0.7) (Bodungen *et al.*, 1986); (b) the proximity between $\delta^{13}C$ values for sediments (–23.7 to –26.1, mean = –25.1) and the values reported by Fischer (1989) for plankton collected in surface waters of BS region (–25 to –27); and (c) the similarities between diatom associations in the sediment (Bárcena *et al.*, 1998) and in the water column (Bodungen *et al.*, 1986; Wefer *et al.*, 1988; 1990; Leventer, 1991).

Explanation for anomalous high surface ages is outlined in Bárcena *et al.*, (1998). Waters around Antarctica have low ^{14}C concentrations due to the supply of C coming from old reservoirs (upwelled old waters and old continental ice melting waters). The carbon contained in these waters is consumed by primary pro-

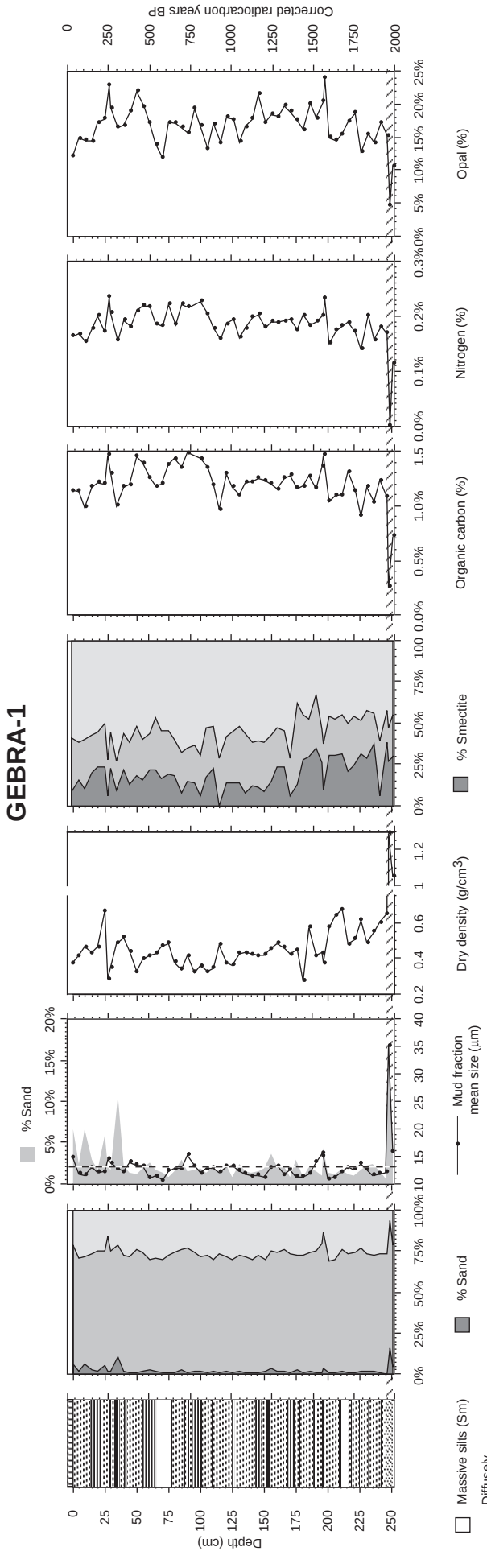

Figure 3 Lithological, sedimentological, mineralogical and geochemical logs of core GEBRA-1. For each log, the left-hand vertical scale represents depth in centimeters and the right-hand vertical scale represents radiocarbon corrected years BP. The two greyed intervals represent the two turbiditic sequences described in the text.

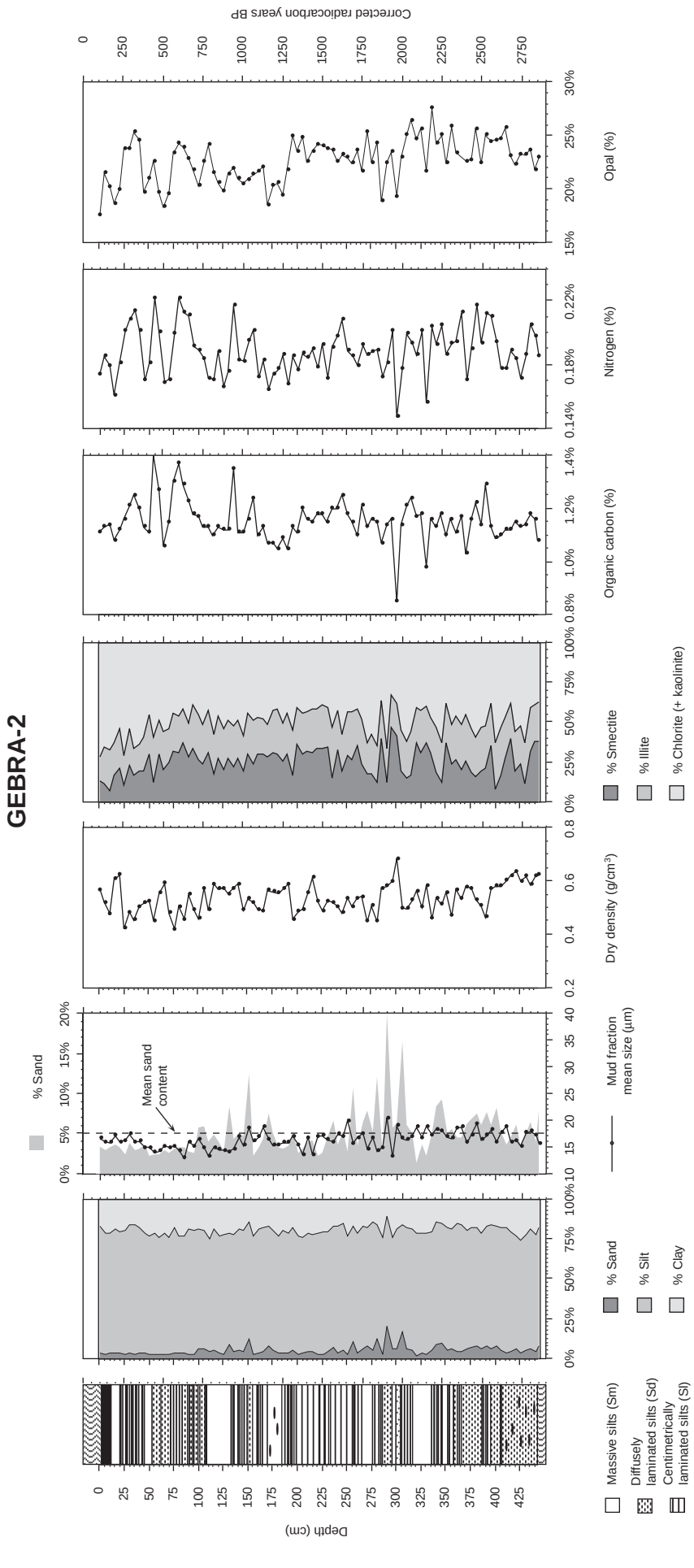

Figure 4 Lithological, sedimentological, mineralogical and geochemical logs of core GEBRA-2. For each log, the left-hand vertical scale represents depth in centimetres and the right-hand vertical scale represents radiocarbon corrected years BP. When comparing organic carbon, nitrogen and opal contents between cores, attention has to be paid to horizontal scales; they are 2.5, 3 and 1.66 times greater in Figure 4 than in Figure 3, respectively.

ducers and therefore the organic matter accumulated at the sea bottom will have a radiocarbon age higher than its actual age. Thus, radiocarbon age has to be corrected to find the real sediment age.

Reservoir-effect correction can be achieved through dating local samples of waters or new organic matter similar to that accumulated in the sediments. Gordon and Harkness (1992) compiled ^{14}C measurements of southern seawater samples and suggested a maximum 1400 years correction. Pudsey and King (1998) suggested a 1430-year correction from the analysis of Northern Weddell Sea sediment trap plankton-rich material.

Even subtracting the maximum reservoir correction (1430 years) derived from sediment trap material to the surface radiocarbon ages of GEBRA-1 and GEBRA-2 cores, corrected surface ages are around 1400 and 1200 years older than expected, respectively. ^{210}Pb and ^{137}Cs results, together with radiocarbon-derived sedimentation rates, indicate that between 5 and 13 cm (*c.* 40–100 years) and a minimum of 16 cm (last *c.* 100 years) could have been lost during the coring process of GEBRA-1 and GEBRA-2, respectively. The almost complete recovery of GEBRA-1 (not more than 13 cm lost) is also confirmed by the brown colour of its first 2 cm. Brown colour is related to the oxidizing character of subsurface sediments, still in contact through the interstitial waters with the overlying oxygenated water mass (Yoon *et al.*, 1994; Calafat *et al.*, 1997). Regarding the similar ^{14}C surface ages obtained in both cores and the recovery method, the maximum amount of material lost in GEBRA-2 may not be substantially more than 16 cm. Anomalous old radiocarbon surface ages in Antarctic marine sediments higher than reservoir correction have been cited in previous works (Harden *et al.*, 1992; Domack *et al.*, 1993; Leventer *et al.*, 1996; Cunningham *et al.*, 1999). Harden *et al.* (1992), using ^{14}C and ^{210}Pb data, attributed mainly to old organic particle resuspension and redeposition at a century scale the anomalous ^{14}C surface ages of AP marine sediments. Despite these high surface ^{14}C ages, they stated that ^{14}C profiles in BB deep sediments are not seriously affected by biological reworking and, thus, the values approximate true rates of sediment accumulation. Therefore sediment accumulation rates have been used to determine the time period represented by the recovered sediments, yielding that GEBRA-1 records the sedimentation in CBB during a period of *c.* 1950 years and GEBRA-2 records the sedimentation in AP slope of EBB during a period of *c.* 2750 years.

Taking into account the points above, using the minimum lost section for both cores and considering constant through time the contamination by old organic particles, the recovered sediments represent the sedimentary record between *c.* 40 and *c.* 1990 years BP in the bottom of CBB and between *c.* 100 and *c.* 2850 years BP in the AP slope of EBB. All the sediment ages cited in the remainder of this discussion and in the logs represented in the figures refer to this age model.

Hemipelagic sedimentation

Most of the recovered sediments, except the lowermost section of GEBRA-1, between 246 cm and the core base, and the section between 302 and 306.5 cm in GEBRA-2, have been interpreted as hemipelagic sediments.

The main sources of fine terrigenous particles to the water column in BB area are: (a) subglacial discharge from tidewater glaciers that feed sediment-laden nepheloid layers (Griffith and Anderson, 1989; Domack and Ishman, 1993; Domack *et al.*, 1994; Yoon *et al.*, 1997); and (b) fluvial discharge from glaciers that end on land and/or supraglacial discharge from ice surface, responsible for the overflow plumes in some SSI bays (Yoon *et al.*, 1998). Fjord morphology and circulation control the dispersal of glacial-derived particles out of the fjords and off coastal waters. Fjords in SSI facing BB have often an estuarine circulation pattern during summer, with an outflow of sediment-laden, fresh surface waters and an inflow of cold deep saline waters coming from the basin (Domack and Ishman, 1993). Once those surface waters reach the fjord mouth they are dispersed northward following the general circulation paths in the basin. Other glacigenic particles such as ice-rafted debris (IRD) reach the basin floor as well. This mode of transportation of coarse particles could explain the sparse presence of particles coarser than 1 mm within the hemipelagic sections. The last source of terrigenous particles is the input of volcanic dust eroded from exposed volcanic surfaces from the surrounding areas or coming directly from the volcanic cones as it seems to be the case for the coarse layers at the top (between 0 and 40 cm) of core GEBRA-1. These layers show a higher content in sand-sized volcanic ash but none of the distinctive pronounced features regarding mean size of mud particles, physical properties and composition of the sandy silt layer identified at the base of the same core and interpreted as turbidity current-related (see following section). Moreover, some of these ash-rich coarse layers correlate with the age of the Deception Island volcanic events around 350 (Aristarain *et al.*, 1990) and 85 years BP (Orheim, 1972). None of the tephra layers recognized in Livingston Island lakes by Björck *et al.* (1991), dated between 450 and 1350 years BP, has been identified in GEBRA-1 core, probably due to a lack of resolution of our subsampling strategy. Conversely, the layers that we identify were not recognized by Björck *et al.* (1991), probably due, as the same authors suggest, to errors in some of the dates from King George Island lakes, the low sedimentation rates in Livingston Island lakes after *c.* 3000 years BP, or unusual dispersal pattern of the tephra.

The second major source of fine particles is surface plankton productivity. BB is biologically very productive during austral summer months when its surface is ice-free. Productivity during this period is quite variable from year to year and one of the highest in the Atlantic sector of the Southern Ocean. Basterretxea and Arístegui (1999) reported primary production integrated values for different areas in BB at two different years (1991 and 1993) ranging from 330 ± 43 to 2673 ± 1754 mg C m^{-2} day^{-1}. Most of the plankton productivity is linked to diatoms and, to a minor extent, to silicoflagellates, all of them presenting opal skeletons.

All these fine (terrigenous and biogenic) particles are transferred through different mechanisms to the deep basin. Sediment trap experiments in CBB, not far from the location of core GEBRA-1 (Figure 1), have shown that vertical particle fluxes during the sea-ice-free months are among the highest in the southern ocean (Wefer *et al.*, 1988; 1990). Nevertheless, the presence of intact frustules in sediment trap material and in the bottom sediments (Bárcena *et al.*, 1998) implies mechanisms other than simply repackaging into faecal pellets. Discrete particles that fall in the water column and incorporation into aggregates should also play a role in the transfer of particles to deep waters (Bodungen *et al.*, 1986; Leventer, 1991). The same sediment trap experiments show that advection from other areas supplies terrigenous and biogenic particles to deep waters during ice-free and even ice-covered periods (Gersonde and Wefer, 1987; Wefer *et al.*, 1988; 1990; Abelmann and Gersonde, 1991).

The comparison of the sediment fluxes and main components abundance (organic matter, opal and terrigenous fraction) obtained from sediment trap experiments in CBB, and estimated from the hemipelagic sections of GEBRA-1 and GEBRA-2 cores (Table 4), reveals striking differences. Annual particle fluxes measured in sediment traps placed around 500 m depth are lower but richer in biogenic components (organic matter and biogenic silica) than those calculated in the hemipelagic sections. The same difference is observed if we compare the estimated fluxes from hemipelagic sediments and the fluxes measured in deeper waters (1588 m depth, 364 m above bottom). Considering that sedimentary dynamics of BB may have not changed substantially during the

Table 4 Measured and estimated fluxes (g/m^2·y), and main components' abundance, in the hemipelagic intervals of cores GEBRA-1 (G-1) and GEBRA-2 (G-2), in the sediment traps and in shelf sediments of the BB. Data on sediment traps and shelf sediments are from (1) Wefer *et al.* (1988), (2) Wefer *et al.* (1990) and (3) DeMaster *et al.* (1987) (for location of sediment traps and shelf sediments' sampling stations, see Figure 1)

Data source	Core or trap identification	Core/trap (bottom) depth (m)	Total	Org. matter	Opal	Terrig.	% org. matter	% opal	% terrig.
Hemipelagic sediments	G-1 (0–246 cm)	1652	577.5	21.1	98.6	457.8	3.65%	17.08%	79.27%
	G-2 (0–244 cm)	1106	869.4	30.0	196.7	642.7	3.45%	22.63%	73.92%
Turb. sed.	G-1 (246–252 cm)	1652					1.47%	7.70%	90.83%
Shallow traps	KG1 (1)	494	120.0	23.0	54.8	42.2	19.88%	47.36%	32.76%
	KG2 (2)	693	11.9	1.1	3.5	7.3	9.24%	29.41%	61.34%
	KG3 (2)	687	36.6	3.3	18.3	15.0	9.02%	50.00%	40.98%
	Mean						12.71%	42.26%	45.03%
Deep trap	KG1 (1)	1588 (1952)	107.2	9.7	38.8	58.7	9.51%	38.04%	52.45%
Shelf sediments	G8601-38 (3)	440					1.35%	3.48%	95.17%
	G8601-52 (3)	452					1.68%	5.98%	92.34%
	G8601-25 (3)	247					1.80%	5.61%	92.59%
	G8601-04 (3)	658					1.80%	7.10%	91.10%
	Mean						1.66%	5.54%	92.80%

last few thousand years (Singer, 1987; Harden *et al.*, 1992), these differences can be explained by lateral near-bottom inputs contributed by nepheloid layers or turbidity currents originating in the shelf break or continental slope.

Figure 5 displays the composition of sediment trap materials, box core surface samples from SSI and AP shelf and upper slope sediments (<700 m), terrigenous coastal particles from surrounding emerged areas and the sediments in our cores (for details and references, see Table 4). Shelf/upper slope sediments' composition falls between the composition of two end members, terrigenous particles coming from the BB borderland and biogenic rich material coming from surface waters. The position of shelf/upper slope sediments, very close to coastal terrigenous particles, shows that shelf/upper slope sediments have an important contribution from terrigenous particles coming from the emerged areas. GEBRA-1 and GEBRA-2 hemipelagic sediments can be regarded as a mixture of particles coming from surface waters, represented by the sediment trap samples (around 30%), and an important contribution of shelf/upper slope particles transported by bottom nepheloid layers (Figure 5) (around 70%).

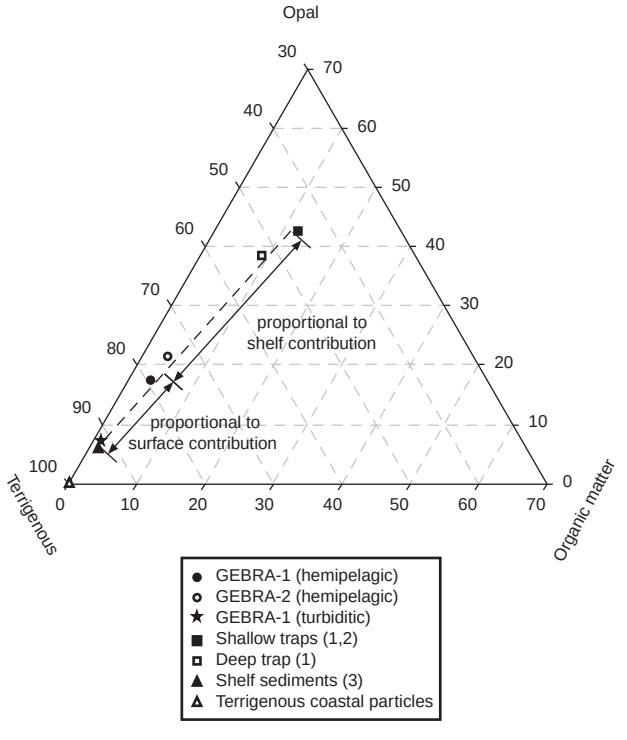

Figure 5 Mean main component ternary diagram of the hemipelagic sections of GEBRA-1 and GEBRA-2, the material collected in sediment traps (1 Wefer *et al.*, 1988; 2 Wefer *et al.*, 1990), shelf sediments surface samples (3 DeMaster *et al.*, 1987) and terrigenous material coming from emerged areas (100% terrigenous). Note the position of the hemipelagic sediments between the material that comes directly from surface waters and material accumulated in shelf areas.

Suspended sediment concentrations in BB shelf areas may be quite high, at least during ice-free periods. This resuspension is due to stirring of the bottom by strong waves during stormy periods, tidal currents (López *et al.*, 1994) and internal waves at density interfaces (García *et al.*, 1994; Calafat *et al.*, 1997). This suspended sediment may be advected off the shelf by ambient currents as the inferred bottom current along the SSI shelf (Yoon *et al.*, 1998) or the inflow of cold and salty Weddell Sea shelf waters around the tip of AP and through Antarctic Sound (Whitworth *et al.*, 1994; López *et al.*, 1999). The importance of resuspension and export processes affecting fine particles accumulated in shelf areas is confirmed by sedimentological, water column (Yoon *et al.*, 1998), subbottom (Jeffers and Anderson, 1990), geochemical (DeMaster *et al.*, 1991) and palaeontological evidence (Rutgers van der Loeff and Berger, 1991). The anomalous high surface ^{14}C ages of the recovered sediments are regarded as another evidence of sediment resuspension and downslope transfer.

The shift in sources of material, pelagic particles settling from surface waters and advected particles from shelf and upper slope, is proposed to explain the laminated nature of the hemipelagic sediments as well. Leventer *et al.* (1996) also attribute dark laminations recognized in hemipelagic sediments from the Palmer Deep, further south in the Pacific margin of the AP, to seasonal inputs of highly biogenic material coming from surface waters. In

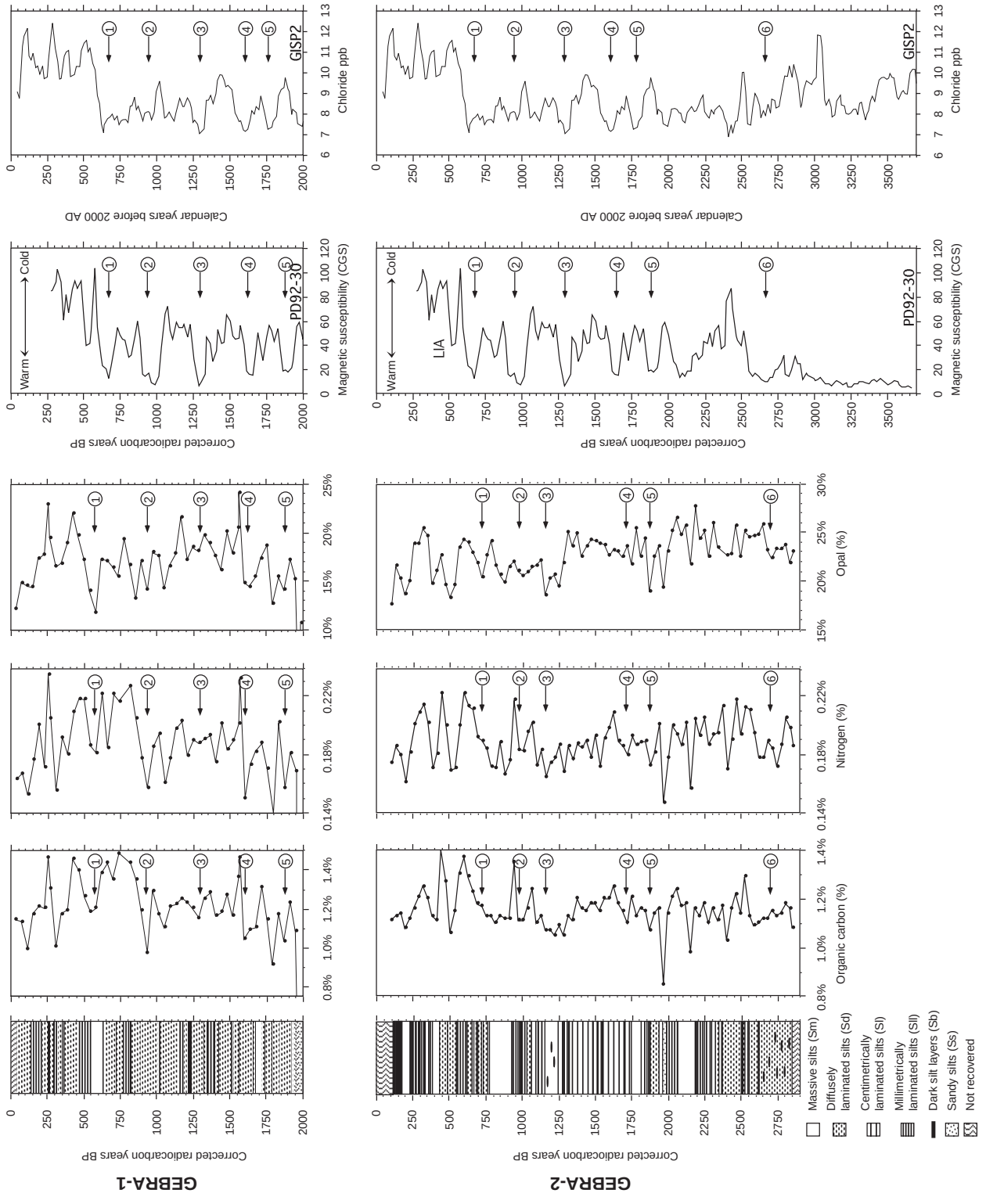

Figure 6 Palaeoclimatic interpretation of lithological and geochemical logs of the hemipelagic sections in GEBRA-1 and GEBRA-2. Magnetic susceptibility log for core PD92-30 and GISP2 chloride log are from Domack and Mayewski (1999) and are used for comparison purposes. The numbers (Domack and Mayewski, 1999) refer to warm events. LIA: 'Little Ice Age'.

our sediments, the decrease in definition of black lamina (from black layers to massive sediments) can be interpreted as a dilution of biogenic material by terrigenous (shelf/upper slope derived) material.

Turbiditic sedimentation

The sediments in the lowermost section of core GEBRA-1 between 246 and 252 cm have been interpreted as turbiditic sediments regarding their distinctive characteristics. These sediments have a very high sand content, high mud fraction mean size, high dry density and low biogenic components content. Holler (1989) and Yoon *et al.* (1994) already attributed a turbiditic origin to sediments with these characteristics recovered in CBB.

The similarity between the composition of turbiditic sediments and shelf/upper slope sediments reinforces (Figure 5) the interpretation of its origin as the turbiditic flows that transported them probably originated in the shelf break or the upper slope, or other areas rich in terrigenous particles as the flanks of the volcanic edifices near the location of core GEBRA-1. In fact, the abundance, morphology and composition of the ashes in this layer (Fabrés, 1998) and the proximity to the steep flanks of the volcanic edifices west and northeast of core GEBRA-1 (Figure 1) suggests these volcanic edifices as the source area for the turbiditic flows. Other authors have identified, through the use of other techniques, deposits corresponding to turbiditic flows in different areas of the CBB (Anderson and Molnia, 1989; Jeffers and Anderson, 1990; Ercilla *et al.*, 1998; Prieto *et al.*, 1999). The high topographic gradients of volcanic edifices (Gràcia *et al.*, 1996) and the important volcanic (Orheim, 1972; Smellie, 1990) and seismic activity (Pelayo and Wiens, 1989) of this area are factors that would favour the initiation of turbiditic flows. The comparison of the composition of the turbiditic layer identified in GEBRA-1 (the fluxes were not calculated since a turbiditic event is considered instantaneous) with the composition of the hemipelagic sediments of both cores and the composition of the particles collected in sediment traps reveals that the contribution of turbidity currents in the hemipelagic sections has to be minor or inexistent since the compositional signature of those events is distinctive and is not clearly found anywhere else.

The abundance of coarse layers between 125 cm and the base of core GEBRA-2 deserves some discussion about the influence of turbiditic sedimentation in the area where GEBRA-2 was recovered. The comparison of sand content and mean size of mud fraction yields some doubt about the actual coarse character of these layers compared to the coarse layer at the base of GEBRA-1. These discrepancies could be the result of the difficulties found in sieving of some samples in GEBRA-2 core due to the abundance of sponge spicules that probably retained some clay and silt fraction despite repeated water rinsing. Moreover, excepting the sandy silt layer between 302 and 306.5 cm depth, that can be interpreted as well as turbidity current-related, none of the coarse layers shows the distinctive characteristics regarding dry density and composition of the CBB turbiditic layer. Furthermore, GEBRA-2 core was recovered near the top of a 300 m high sediment mound located at the foot of a 600 m high scarp (see Figure 2 in Bárcena *et al.* 1998) and genetically related tentatively by Canals and GEBRA '93 Team (1993) to the activity of bottom currents. This mound can be physiographically compared, despite different time and dimension scales, with the sediment drifts located further south in the AP margin. The genesis of these drifts has been traditionally related to the interaction between turbiditic flows and bottom currents (Rebesco *et al.*, 1997). Pudsey and Camerlenghi (1998) concluded that at least during their last stage those sediment drifts were maintained by the supply of particles transported by bottom nepheloid layers fed by pelagic settling and turbid meltwater plumes, while turbiditic flows would predominate mostly during glacials. A similar situation could be responsible for the accumulation of hemipelagic sediments in the mound where GEBRA-2 was obtained, given that, due to the proximity to the shelf and lower depth of this setting, the bottom nepheloid layer could be nourished with bigger amounts of terrigenous and biogenic particles during the interglacial periods, including the Holocene. This fact would also explain the higher sedimentation rates of this area compared to the CBB.

Turbiditic flows have no influence in the age model proposed for core GEBRA-1 since the oldest dated sample lies above the turbiditic section, and only a very limited influence in GEBRA-2 because of the minor thickness of the turbiditic section compared to the hemipelagic sediment pile. Moreover, the slope of the depth-age curve between the surface and mid-core dated samples, and between the mid-core and the lowest dated sample (where the turbiditic section is), is practically equal.

Palaeoceanographic and palaeoclimatic interpretation

Our investigation of sedimentary processes responsible for the accumulation of GEBRA-1 and GEBRA-2 hemipelagic sediments allows us to establish the relation between surface oceanographic conditions and the chemical composition of the sediments accumulated in the basin floor.

Climatic and oceanographic control on the composition of hemipelagic sediments

During warm periods the amount of terrigenous particles entrained in the marine environment by epi-, sub- and pro-glacial meltwater will increase substantially. Moreover, during warm periods with a longer sea-ice-free season, resuspension in shelf and shelf break areas is enhanced. Finally, deep circulation in BB, and thus the activity of bottom nepheloid layers, may also be enhanced during warm periods. Pudsey (1992) stated that formation of Weddell shelf waters was enhanced during past interglacial periods due to the increased melting and recirculation under ice shelves because of larger floating areas. The same kind of inference can be applied during the smoother climatic fluctuations of the last few thousand years. Warm periods would, as well, be characterized by enhanced formation and flow of shelf waters to the deep BB and, thus, resuspended particles from shelf and shelf break would be more efficiently transported to deeper areas. The increased circulation of oxygenated and silica-undersaturated shelf waters would also produce oxidation of organic matter and dissolution of biogenic silica in deep sediments.

Factors controlling spring phytoplankton blooms responsible for the entrance of biogenic rich matter from surface waters are still under debate. The opening and melting of sea ice is, as shown by sediment trap experiments in areas covered seasonally by sea ice, a determinant factor in surface productivity since it allows the entrance of light in the upper water column (Wefer *et al.*, 1988; Abelmann and Gersonde, 1991; Abelmann, 1992; Dunbar *et al.*, 1998). Phytoplankton blooms would not develop under permanent sea-ice cover and, thus, cold periods with permanent or quasi-permanent sea ice would lead to a substantial decrease in the flux of biogenic components from surface waters. The same sediment trap experiments have shown that mid-water particle fluxes are more related to bloom development favoured by the formation of a shallow surface mixed layer than to the length of the sea-ice-free season (Leventer, 1991; Mitchell and Holm-Hansen, 1991; Abelmann, 1992; Leventer *et al.*, 1996). Formation of a shallow surface mixed layer is related, among others, to: (a) fast melting of sea ice over a wide area (Smith and Nelson, 1985; Fischer *et al.*, 1988); (b) higher spring and summer temperatures (Leventer, 1991); and (c) reduced spring and summer windiness (Dunbar *et al.*, 1998). Elevated biogenic content and high abundance of *Chaetoceros* resting spores throughout the studied sediments (Bárcena *et al.*, 1998) suggests that, despite slight climatic

fluctuations, conditions favouring phytoplankton blooms have occurred repeatedly during the warmer season in BB during the last three millennia.

Climatic evolution of the last three millennia

Taking into account the processes that contribute sedimentary particles to deep areas and the relation between geochemistry and micropaleontological assemblages (Bárcena *et al.*, 1998), terrigenous versus biogenic content of BB deep sediments seems to be more influenced by the fluctuations in input and transfer to deep areas of terrigenous particles than by fluctuations in surface primary productivity. Then, epochs characterized by the accumulation of massive or diffusely laminated sediments with high terrigenous content can be interpreted as periods with warm conditions, while epochs characterized by laminated sediments with high biogenic contents can be interpreted as cold periods (Figure 6). The main difference between this climate-controlled model and the model proposed by Leventer *et al.* (1996) for the Palmer Deep is that they interpret periods with increased biogenic content as warm periods. The explanation for this lies on the almost total absence of meltwater from the glaciers that surround Palmer Deep (Griffith and Anderson, 1989). Consequently, the terrigenous input from Palmer Deep surrounding emerged areas plays a minor role in controlling sediment composition and, in contrast with BB, fluctuations in surface-water productivity, probably more dramatic due to its southern position, control sediment geochemistry.

Bárcena *et al.* (1998) already proposed a first interpretation of the evolution of environmental conditions for the last three millennia in BS. They interpreted periods with high abundance of Sea Ice Taxa as cold periods and found a relation between their cold periods and global fluctuations of alpine glaciers (Wigley and Kelly, 1990). The analysis of geochemical data (organic carbon, nitrogen and biogenic silica) of the hemipelagic sections of GEBRA-1 and GEBRA-2 allows us to identify a series of climatic pulses as well. The pulses identified show great resemblance to those identified by Leventer *et al.* (1996) in Palmer Deep using magnetic susceptibility logs in sediments (core PD92–30) similar to those that we have studied in the BB (Figure 6). The relation of the record in core PD92-30 with global ocean circulation has been recently postulated by Domack and Mayewski (1999), who identified similarities with the GISP2 ice-core record from Greenland (Figure 6).

In Figure 6 we compare records from cores PD92–30 and GISP2 with the organic carbon, nitrogen and opal records of our GEBRA-1 and GEBRA-2 cores. The most outstanding climatic pulse features are common both to the Palmer Deep record (Leventer *et al.*, 1996) and to our records in the BB. Cooling at the onset of the 'Little Ice Age' (LIA) (just above number one in Figure 6) and the fluctuations inside this period (LIA) can be correlated to all our biogenic records, especially in GEBRA-2 core. The correlation in GEBRA-1 is not as good as in GEBRA-2, probably due to the lower temporal resolution of the former and, perhaps, to a stronger influence of oxidation and dissolution by deep circulation of shelf waters. The outstanding character of the climatic pulses lying within the LIA has also been remarked upon by Barker *et al.* (1998). The adjustment eventually needed to obtain the best fit between the ages of the climatic events in GEBRA-1 and GEBRA-2 and in PD92-30 and GISP2 records falls within the error range of the radiocarbon dating method and the probable fluctuations of the sedimentation rates between two dated points. Some, but not all, of the 200–300 year fluctuations identified by Leventer *et al.* (1996) between 2850 years BP and the onset of the LIA can also be identified in our records. In some cases, the warm intervals between two cold periods are very short (less than 100 years) and their identification in a record with less than decade resolution can be difficult, as is the case for the warm interval around 1700 years BP (warm event labelled with number four). Additionally, those that are not so well correlated (warm event two) correspond to the fluctuations that are not so well represented in the GISP2 ice-core record either (Domack and Mayewski, 1999). Thus, these fluctuations have probably a local Palmer Deep climate imprint that may not be completely uniform in the whole western side of AP.

All the parallels identified between our records and those of Palmer Deep and GISP2 demonstrate that deep fine-grained sediments from BB contain a high-resolution record of global climatic fluctuations during the late Holocene.

Conclusions

Sediments recovered in cores GEBRA-1 and GEBRA-2 record sedimentary processes and oceanographic conditions from ≈1990 to ≈40 years BP in the CBB and from ≈2850 to ≈100 years BP in the EBB. The elevated sedimentation rates in the deep parts of BB result from high amounts of fine particles released both from onshore and shallow water sources, and biogenically produced in the upper layer of the water column. Because of its general physiography, the BB acts as a giant sediment trap.

Hemipelagic settling and turbiditic sedimentation, to a minor extent, have dominated sediment accumulation in the floor of CBB during the last two millennia and in the AP slope of EBB during the last three millennia.

Palaeoceanographic and palaeoclimatic interpretation of the hemipelagic sediments allows the identification of the main late-Holocene climatic events, the 'Little Ice Age', and other less dramatic climate fluctuations with a 200–300 year frequency.

Fine-grained sediments on the floor of BB have proved to record accurately the global palaeoclimatic evolution during the late Holocene.

Acknowledgements

We thank the officers and the crew of *Hespérides* for their collaboration during GEBRA '93 cruise. We also want to thank Dr Guillermo Francés for core description, the Scientific-Technical Services (SCT) of the University of Barcelona for their help in mineralogical and geochemical analyses, Dr Pere Masqué for helping in interpreting ^{14}C, ^{210}Pb and ^{137}Cs data, and Drs Eugene W. Domack and Michele Rebesco for their useful review of the original manuscript. The Spanish research projects belonging to the Spanish Antarctic Research Program ANT93-1008-C03-01, ANT93-1008-C03-03 and ANT97-1958-E supported this research. GRC Geociències Marines has also received financial support from 'Comissionat d'Universitats i Recerca de la Generalitat de Catalunya' through grant SGR99/63. The research presented in this paper has also been supported by cooperative project 99120 from 'Comisión de Intercambio Cultural Educativo y Científico entre España y los Estados Unidos de América'. JF thanks the Spanish Education Ministry for the PhD grant (AP95 44002743).

References

Abelmann, A. 1992: Radiolarian flux in Antarctic waters (Drake Passage, Powell Basin, Bransfield Strait). *Polar Biology* 12, 357–72.

Abelmann, A. and **Gersonde, R.** 1991: Biosiliceous particle flux in the Southern Ocean. *Marine Chemistry* 35, 503–36.

Anderson, J.B. and **Molnia, B.F.** 1989: Glacial-marine sedimentation: Short course in geology. 28th International Geological Congress, Washington DC, American Geophysical Union, 233–65.

Aristarain, A.J., Jouzel, J. and **Lorius, C.** 1990: A 400 years isotope record of the Antarctic Peninsula climate. *Geophysical Research Letters* 17, 2369–72.

Banfield, L.A. and **Anderson, J.B.** 1995: Seismic facies investigation of the Late Quaternary glacial history of Bransfield Basin, Antarctica. In Cooper, A.K., Barker, P.F., Webb, P.N. and Brancolini, G., editors, *Geology and seismic stratigraphy of the Antarctic margin*, Washington DC: American Geophysical Union, 123–40.

Bárcena, M.A., Gersonde, R., Ledesma, S., Fabrés, J., Calafat, A.M., Canals, M., Sierro, F.J. and **Flores, J.A.** 1998: Record of Holocene glacial oscillations in the Bransfield Basin as revealed by siliceous microfossil assemblages. *Antarctic Science* 10, 269–85.

Barker, P.F., Barret, P.J., Camerlenghi, A., Cooper, A.K., Davey, F.J., Domack, E.W., Escutia, C., Kristoffersen, Y. and **O'Brien, P.E.** 1998: Ice sheet history from Antarctic continental margin sediments: the ANTOSTRAT approach. *Terra Antarctica* 5, 737–60.

Basterretxea, G. and **Arístegui, J.** 1999: Phytoplankton biomass and production during late austral spring (1991) and summer (1993) in the Bransfield Strait. *Polar Biology* 21, 11–22.

Biscaye, P.E. 1965: Mineralogy and sedimentation of recent deep-sea clay in the Atlantic Ocean and adjacent seas and oceans. *Geological Society of America Bulletin* 76, 803–32.

Björck, S., Sandgren, P. and **Zale, R.** 1991: Late Holocene tephrochronology of the Northern Antarctic Peninsula. *Quaternary Research* 36, 322–28.

Bodungen, B.V., Smetacek, V.S., Tilzer, M.M. and **Zeitschel, B.** 1986: Primary production and sedimentation during spring in the Antarctic Peninsula region. *Deep-Sea Research* 33, 177–94.

Boyce, R.E. 1976: Definitions and laboratory determination of compressional sound velocity parameters and wet-water content, wet-bulk density and porosity parameters by gravimetric and gamma-ray attenuation techniques. In Schlanger, S.O., Jackson, E.D. Boyce, R.E., Cook, H.E., Jenkyns, H.C., Johnson, D.A., Kaneps, A.G., Kelts, K.R., Martini, E., McNulty, C.L. and Winterer, E.L., *Initial Reports of the Deep Sea Drilling Project*, 33, Washington: US Government Printing Office, 931–58.

Calafat, A., Durrieu de Madron, X. and **Canals, M.** 1997: Registro contínuo de las variaciones de temperatura del agua de fondo en un volcán submarino (Estrecho de Bransfield, Antártida). *Boletín de la Real Sociedad Española de História Natural* (Sección Geología) 93, 63–71.

Canals, M. and **GEBRA '93 Team** 1993: Evolución geológica de la Cuenca de Bransfield y de la Dorsal Sur del Mar Scotia. Universidad de Barcelona, Cruise report, 176 pp.

Crowley, T.J. and **Baum, S.K.** 1995: Is the Greenland Ice Sheet bistable? *Paleoceanography* 10, 357–63.

Cunningham, W.L., Leventer, A., Andrews, J.T., Jennings, A.E. and **Licht, K.J.** 1999: Late Pleistocene-Holocene marine conditions in the Ross Sea, Antarctica: evidence from the diatom record. *The Holocene* 9, 129–39.

DeMaster, D.J., Nelson, T.M., Harden, S.L. and **Nittrouer, C.A.** 1991: The cycling and accumulation of biogenic silica and organic carbon in Antarctic deep-sea and continental margin environments. *Marine Chemistry* 35, 489–502.

DeMaster, D.J., Nelson, T.N., Nittrauer, C.A. and **Harden, S.L.** 1987: Biogenic silica and organic carbon accumulation in modern Bransfield Strait sediments. *Antarctic Journal of the United States* 22, 108–10.

Domack, E.W. and **Ishman, S.** 1993: Oceanographic and physiographic controls on modern sedimentation within Antarctic fjords. *Geological Society of America Bulletin* 105, 1175–89.

Domack, E.W. and **Mayewski, P.A.** 1999: Bi-polar ocean linkages: evidence from late-Holocene Antarctic marine and Greenland ice-core records. *The Holocene* 9, 247–51.

Domack, E.W., Foss, D.J.P., Syvitski, J.P.M. and **McClennen, C.E.** 1994: Transport of suspended particulate matter in an Antarctic fjord. *Marine Geology* 121, 161–70.

Domack, E.W., Mashiotta, T.A., Burkley, L.A. and **Ishman, S.** 1993: 300-year cyclicity in organic matter preservation in Antarctic fjord sediments. In Kennett, J.P., Warnke, D.A., editors, *The Antarctic paleoenvironment: a perspective on global change*, Washington DC: Antarctic Research Series 60, 265–72.

Dunbar, R.B., Leventer, A.R. and **Mucciarone, D.A.** 1998: Water column sediment fluxes in the Ross Sea, Antarctica: atmospheric and sea ice forcing. *Journal of Geophysical Research* 103, 30741–59.

Ercilla, G., Baraza, J., Alonso, M. and **Canals, M.** 1998: Recent geological processes in the Central Bransfield Basin (Western Antarctic Peninsula). In Stoker, M.S., Evans, D. and Cramps, A., editors, *Geological processes on continental margin sedimentation, mass-wasting and stability*, London: Geological Society of London Special Publication 129, 205–16.

Fabrés, J. 1998: Sedimentología y paleoceanografía del Holoceno reciente de la Cuenca de Bransfield (Antártida Occidental). Ms thesis, University of Barcelona, 129 pp.

Fischer, G. 1989: Stabile kohlenstoff-isotope in partikularer organisher substanz aus dem sudpolrmeer (Atlantischer secktor). PhD dissertation, University of Bremen, 161 pp.

Fischer, G., Fütterer, D., Gersonde, R., Honjo, S., Ostermann, D. and **Wefer, G.** 1988: Seasonal variability of particle flux in the Weddell Sea and its relation to ice cover. *Nature* 335, 426–28.

García, M.A., López, O., Sospedra, J., Espino, M., Gràcia, V., Morrison, G., Rojas, P., Figa, J., Puigdefàbregas, J. and **Sánchez-Arcilla, A.** 1994: Mesoscale variability in the Bransfield Strait region (Antarctica) during Austral summer. *Annales Geophysicae* 12, 856–67.

Gersonde, R. and **Wefer, G.** 1987: Sedimentation of biogenic siliceous particles in Antarctic waters from the Atlantic sector. *Marine Micropaleontology* 11, 311–32.

Gordon, J.E. and **Harkness, D.D.** 1992: Magnitude and geographic variation of the radiocarbon content in Antarctic marine life: Implications for reservoir corrections in radiocarbon dating. *Quaternary Science Reviews* 11, 697–708.

Gràcia, E., Canals, M., Farràn, M., Prieto, M.J., Sorribas, J. and **GEBRA '93 Team.** 1996: Morphostructure and evolution of the Central and Eastern Bransfield basins (NW Antarctic Peninsula). *Marine Geophysical Researches* 18, 429–48.

Gràcia, E., Canals, M., Farràn, M., Sorribas, J. and **Pallàs, R.** 1997: Central and Eastern Bransfield Basins (Antarctica) from high-resolution swath-bathymetry data. *Antarctic Science* 9, 168–80.

Griffith, T.W. and **Anderson, J.B.** 1989: Climatic control of sedimentation in bays and fjords of the northern Antarctic Peninsula. *Marine Geology* 85, 181–204.

Grim, R.E. 1953: *Clay mineralogy*. London: McGraw-Hill.

Grobe, H. and **Mackensen, A.** 1992: Late Quaternary climatic changes as recorded in sediments from the Antarctic continental margin. In Kennett, J.P. and Warnke, D.A., editors, *The Antarctic paleoenvironment: a perspective on global change*, Washington DC: American Geophysical Union, 349–76.

Harden, S.L., DeMaster, D.J. and **Nittrouer, C.A.** 1992: Developing sediment geochronologies for high-latitude continental shelf deposits: a radiochemical approach. *Marine Geology* 103, 69–97.

Holler, P. 1989: Mass physical properties of sediments from Bransfield Strait and Northern Weddell Sea. *Marine Geotechnology* 8, 1–18.

Jeffers, J.D. and **Anderson, J.B.** 1990: Sequence stratigraphy of the Bransfield Basin, Antarctica: implications for tectonic history and hydrocarbon potential. In John, B.S., editor, *Antarctica as an exploration frontier: hydrocarbon potential, geology and hazards*, Tulsa: AAPG Studies in Geology, 13–29.

Leventer, A. 1991: Sediment trap diatom assemblages from the northern Antarctic Peninsula region. *Deep-Sea Research* 38, 1127–43.

Leventer, A., Domack, E.W., Ishman, S.E., Brachfeld, S., McClennen, C.E. and **Manley, P.** 1996: Productivity cycles of 200–300 years in the Antarctic Peninsula region: understanding linkages among the sun, atmosphere, oceans, sea ice, and biota. *GSA Bulletin* 108, 1626–44.

López, O., García, M.A., Gomis, D., Rojas, P., Sospedra, J. and **Sánchez-Arcilla, A.** 1999: Hydrographic and hydrodinamic characteristics of the eastern basin of the Bransfield Strait (Antarctica). *Deep-Sea Research* I46, 1755–78.

López, O., García, M.A. and **Sánchez-Arcilla, A.** 1994: Tidal and residual currents in the Bransfield Strait. *Annales Geophysicae* 12, 887–902.

Manley, P. 1996: Productivity cycles of 200–300 years in the Antarctic Peninsula region: understanding linkages among the sun, atmosphere, oceans, sea ice, and biota. *Geological Society of America Bulletin* 108, 1626–44.

Mitchell, B.G. and **Holm-Hansen, O.** 1991: Observations and modelling of the Antarctic phytoplankton crop in relation to mixing depth. *Deep-Sea Rearch* 38, 981–1007.

Mortlock, R.A. and **Froelich, P.N.** 1989: A simple method for the rapid

determination of biogenic opal in pelagic marine sediments. *Deep-Sea Research* 36, 1415–26.

Niiler, P.P., Amos, A. and **Jian-Hwa, H.** 1991: Water masses and 200 m relative geostrophic circulation in the western Bransfield Strait region. *Deep-Sea Research* 38, 943–59.

Orheim, O. 1972: Volcanic activity on Deception Island, South Shetland Islands. In Adie, R.J., editor, *Antarctic Geology and Geophysics*, Oslo: International Union of Geological Sciences, Series B1, 117–20.

Paterson, S.L. and **Sievers, H.A.** 1980: The Weddell-Scotia confluence. *Journal of Physical Oceanography* 10, 1584–610.

Pelayo, A.M. and **Wiens, D.A.** 1989: Seismotectonics and relative plate motions in the Scotia Sea region. *Journal of Geophysical Researches* 94, 7293–320.

Prieto, M.J., Ercilla, G., Canals, M. and **De Batist, M.** 1999: Seismic stratigraphy of the Central Bransfield Basin (NW Antarctic Peninsula). Interpretation of deposits and sedimentary processes in a glacio-marine environment. *Marine Geology* 157, 47–68.

Prieto, M.J., Gràcia, E., Canals, M., Ercilla, G. and **De Batist, M.** 1997: Sedimentary history of the Central Bransfiled Basin (NW Antarctic Peninsula). The Antarctic Region: Geological Evolution and Processes. Proc. VII ISAES, Siena, 711–17.

Pudsey, C.J. 1992: Late Quaternary changes in Antarctic Bottom Water velocity inferred from sediments grain size in the northern Weddell Sea. *Marine Geology* 107, 9–33.

Pudsey, C.J. and **Camerlenghi, A.** 1998: Glacial-interglacial deposition on a sediment drift on the Pacific margin of the Antarctic Peninsula. *Antarctic Science* 10, 286–308.

Pudsey, C.J. and **King, P.** 1998: Particle fluxes, benthic processes and palaeoenvironmental record in the Northern Weddell Sea. *Deep-Sea Research* I44, 1841–76.

Rebesco, M., Larter, R.D., Barker, P.F., Camerlenghi, A. and **Vanneste, L.E.** 1997: History of sedimentation on the continental rise west of the Antarctic Peninsula. In Cooper, A.K. and Barker, P.F. editors, *Geology and seismic stratigraphy of the Antarctic margin II*, Washington DC: American Geophysical Union, 28–49.

Rutgers van der Loeff, M.M. and **Berger, G.W.** 1991: Scavenging and particle flux: seasonal and regional variations in the Southern Ocean (Atlantic sector). *Marine Chemistry* 35, 553–67.

Singer, J.K. 1987: Terrigenous, biogenic, and volcanoclastic sedimentation patterns of the Bransfield Strait and bays of the northern Antarctic Peninsula: implications for the Quaternary glacial history. PhD dissertation, Rice University, 342 pp.

Smellie, J.L. 1990: Graham Land and South Shetland Islands. In LeMansurier, W.E. and Thomson, J.W., editors, *Volcanoes of the Antarctic Plate and Southern Oceans*, Washington DC: American Geophysical Union, 303–59.

Smith, W.O. and **Nelson, D.M.** 1985: Phytoplankton bloom produced by a receding ice edge in the Ross Sea: Spatial coherence with the density field. *Science* 227, 163–66.

Van der Borg, K., Alderliesten, C., Houston, C.M., De Jong, A.F.M. and **Van Zwol, N.A.** 1987: Accelerator mass spectrometry with ^{14}C and ^{10}Be in Utrecht. *Nuclear Instruments and Methods in Physics Research* B29, 143–45.

Wefer, G., Fischer, G., Fütterer, D. and **Gersonde, R.** 1988: Seasonal particle flux in the Bransfield Strait, Antarctica. *Deep-Sea Research* 35, 891–98.

Wefer, G., Fischer, G., Fütterer, D.K., Gersonde, R., Honjo, S. and **Ostermann, D.** 1990: Particle sedimentation and productivity in Antarctic waters of the Atlantic sector. In Bleil, U. and Thiede, J., editor, *Geological history of the polar oceans: Arctic versus Antarctic*, Dordrecht: Kluwer, 363–79.

Whitworth T. III, Nowlin Jr., W.D., Orsi, A.H., Locarnini, R.A. and **Smith, S.G.** 1994: Weddell Sea shelf water in the Bransfield Strait and Weddell-Scotia Confluence. *Deep-Sea Research* I41, 629–41.

Wigley, T.M.L. and **Kelly, P.M.** 1990: Holocene climatic change, ^{14}C wiggles and variations in solar irradiance. *Philosophical Transactions of the Royal Society of London* 330, 547–60.

Yoon, H.I., Han, M.W., Park, B.K., Han, S.J. and **Oh, J.K.** 1992: Distribution, provenance, and dispersal pattern of clay minerals in surface sediments, Bransfield Strait, Antarctica. *Geo-Marine Letters* 12, 223–27.

Yoon, H.I., Han, M.W., Park, B.K., Oh, J.K. and **Chang, S.K.** 1994: Depositional environment of near surface sediments, King George Basin, Bransfield Strait, Antarctica. *Geo-Marine Letters* 14, 1–9.

—— 1997: Glaciomarine sedimentation and paleo-glacial setting of Maxwell Bay and its tributary embayment, Marian Cove, South Shetland Islands, West Antarctica. *Marine Geology* 140, 265–82.

Yoon, H.I., Park, B.K., Domack, E.W. and **Kim, Y.** 1998: Distribution and dispersal pattern of suspended particulate matter in Maxwell Bay and its tributary, Marian Cove, in the South Shetland Islands, West Antarctica. *Marine Geology* 152, 261–75.